Available online at www.sciencedirect.com
ScienceDirect
Trans. Nonferrous Met. Soc. China 34(2024) 108−121
Transactions of Nonferrous Metals Society of China
www.tnmsc.cn

Microstructure, mechanical and tribological properties of APC/Al laminated composites prepared by hydrothermal carbon adsorption on plates

Yi-han CHEN[1], Hong-yu XU[1,2], Bo JIANG[1], Ye WANG[1], Mao-liang HU[1], Ze-sheng JI[1]

1. School of Materials Science and Chemical Engineering, Harbin University of Science and Technology, Harbin 150080, China;
2. Key Laboratory of Advanced Manufacturing and Intelligent Technology, Ministry of Education, Harbin University of Science and Technology, Harbin 150080, China

Received 27 June 2022; accepted 20 March 2023

Abstract: Amorphous carbon (APC)/Al laminated composites were prepared by hydrothermal carbon adsorption on plates (HTCAP) and vacuum hot-press sintering process. The effect of the glucose solution concentration on the microstructure, mechanical properties and tribological properties was investigated. The results indicate that APC is uniformly distributed between layers and has good interfacial bonding with the matrix through the diffusion of Al. As the glucose solution concentration increases, the interlayer hardness, ultimate tensile strength and elongation first increase and then decrease, while the wear rate shows the opposite trend and the coefficient of friction (COF) gradually decreases. A maximum elongation of 16.4% and a minimum wear rate of 0.344×10^{-5} mm^3/(N·m) are achieved at a glucose solution concentration of 0.3 mol/L. Adhesive wear is the dominant wear mechanism of APC/Al laminated composites. The improvement in wear resistance is attributed to the formation of uniform APC lubrication film on the wear surface.

Key words: Al matrix laminated composites; amorphous carbon; hydrothermal reaction; interfacial microstructure; tribological property

1 Introduction

As the most widely used nonferrous metal structural materials, aluminum and aluminum alloys have the advantages of high specific strength and stiffness, excellent corrosion resistance, high recycling rate and good plasticity processing performance. They have been widely applied in many fields necessary for national development, such as the automotive and aerospace industries [1−3]. However, the disadvantages of aluminum alloys, such as relatively poor wear resistance, limit their further application in high-performance tribological fields. Therefore, reinforcement and lubricating materials have been introduced to prepare aluminum matrix composites (AMCs) and improve the wear resistance of aluminum alloys [4−6].

Recently, carbonaceous materials, such as graphite [7−9], graphene [10−12], and carbon nanotubes (CNTs) [13−15], have been applied to enhancing the wear resistance of aluminum alloys. BARADESWARAN and PERUMAL [16] prepared 7075 aluminum alloy−graphite composites through a conventional liquid casting technique and found that graphite can effectively reduce the coefficient of friction and wear rate of 7075 aluminum alloy, while the hardness and flexural strength of the composites decreased with increasing graphite content. MAURYA et al [17] fabricated Al6061−

Corresponding author: Hong-yu XU, Tel: +86-13069720734, E-mail: xuhongyu@hrbust.edu.cn
DOI: 10.1016/S1003-6326(23)66385-X

graphene composites by a friction stir process, achieving increase in the surface hardness and tribological properties of 160% and 84.2%, respectively. BASTWROS et al [18] prepared Al−CNTs composites via high-energy ball milling, cold compaction and hot extrusion. The results indicated that the wear rate of the Al−5wt.%CNTs composites decreased by 78.8% compared to that of pure aluminum because CNTs were crushed into a carbon film that covered the surface and acted as a solid lubricant, significantly improving the wear behavior.

Although these carbonaceous materials can effectively improve the wear resistance of aluminum alloys, it is still difficult to resolve the problem of uneven dispersion of carbonaceous materials and weak interfacial bonding in aluminum matrix composites by powder metallurgy techniques and casting technique. HE et al [19] proposed a process of hydrothermal carbonized deposition on chips to prepare amorphous carbon (APC)/Al composites and found that amorphous carbon was uniformly distributed in the composites and well bonded with the aluminum matrix interfacially. Moreover, the wear resistance of the composites was significantly improved due to the self-lubricating characteristic of amorphous carbon. Thus, compared with other carbon materials, APC is also a viable material for enhancing the wear resistance of composites, with the advantages of a simple preparation process, an extensive selection range of raw materials, a low cost and a high yield [20,21].

However, the hardness, strength and plasticity of APC/Al composites were gradually reduced [22,23]. A novel kind of bioinspired metal-reinforced laminated composite was designed and fabricated to obtain excellent comprehensive properties. LI et al [24] prepared graphene/aluminum composites with a bioinspired nano-laminated structure by flake powder metallurgy. The results showed that tensile strength and elastic modulus increased by 50% and 20.2%, respectively. The laminated structure can improve the strength and toughness of materials simply and effectively, balance the contradiction between the plasticity and strength of the reinforcement phase and the matrix alloy, and make full use of the mechanical properties of the two different materials.

Therefore, a novel method, called the hydro-thermal carbon adsorption on plates (HTCAP) and vacuum hot-press sintering (VHPS) process, was proposed to prepare APC/Al laminated composites in this work. Then, the effect of the glucose solution concentration on the microstructure, mechanical properties and tribological properties of the APC/Al laminated composites was investigated. Finally, the wear resistance mechanism of the laminated composites was discussed.

2 Experimental

2.1 Primary materials

An industrial A6061 aluminum alloy sheet and glucose crystal powder ($C_6H_{12}O_6·H_2O$, 198.17 g/mol) were used as raw materials for the experiment, and the chemical composition of the A6061 aluminum alloy is given in Table 1. The A6061 aluminum alloy sheet was wire-cut into thin circular plates (d 24 mm × 0.4 mm) with a flat surface. The A6061 plates were ultrasonically cleaned in alcohol for 20 min to remove surface impurities. Meanwhile, glucose crystal powder was added to distilled water and ultrasonically stirred for 10 min to obtain glucose solutions with concentrations of 0.1, 0.2, 0.3 and 0.4 mol/L, respectively.

Table 1 Chemical composition of A6061 aluminum alloy (wt.%)

Mg	Si	Fe	Cu	Zn	Mn	Ti	Cr	Al
1.0	0.7	0.4	0.25	0.25	0.15	0.15	0.2	Bal.

2.2 Preparation process of APC/Al laminated composites

A schematic diagram of the preparation process of the APC/Al laminated composites is shown in Fig. 1. First, the A6061 plates (15 pieces) and glucose solutions (70 mL) with different concentrations were combined in a high-temperature and high-pressure hydrothermal reaction kettle. Then, the sealed reaction kettle was put into a heating furnace for 3 h at 180 °C (hydrothermal reaction). Subsequently, the reaction kettle was cooled to room temperature, and the A6061 plates were taken out and dried at 90 ℃ for 2 h (drying). Afterward, the A6061 plates were heated at 500 ℃ for 2 h in a vacuum thermal furnace (vacuum heating). According to different glucose solution concentrations, the A6061 plates treated by HTCAP process were named HTCAP-0.1,

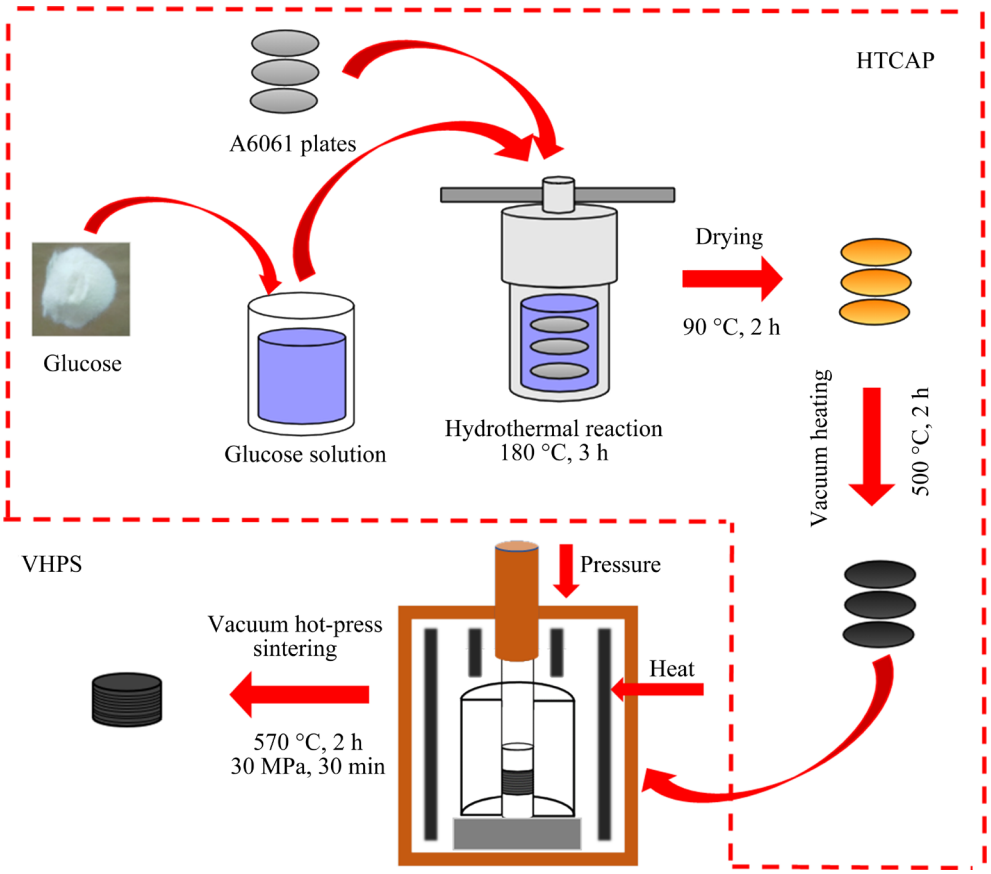

Fig. 1 Schematic diagram of preparation process of APC/Al laminated composites

HTCAP-0.2, HTCAP-0.3 and HTCAP-0.4, respectively. Finally, the A6061 plates (26 pieces) were loaded into a graphite mold with an inner diameter of 24.1 mm, heated at 570 °C for 2 h, and hot-pressed into a billet at a pressure of 30 MPa for 30 min in a vacuum hot-press sintering (VHPS) furnace. Meanwhile, the A6061 plates not treated by the HTCAP process were also subjected to the VHPS process to obtain comparison samples.

2.3 Characterization

Scanning electron microscopy (SEM, FEI Quanta 200 kV) equipped with energy dispersive spectroscopy (EDS) was used to observe the surface morphology of A6061 aluminum alloy plates, the interface morphology of APC/Al laminated composites, and the wear surface morphology of different samples. The thin circular plates of A6061 aluminum alloy treated by the HTCAP process were examined by a Raman spectrometer (HR−800). The microstructure of the composites was observed using an optical microscope (OM, LCMS301). Phase analysis was conducted via X-ray diffraction (XRD, X-Pert PRO). The microstructure of APC and the interfaces of the APC/Al laminated composites were investigated by transmission electron microscopy (TEM/HRTEM, JEM−2100). A room-temperature tensile test was performed at a velocity of 1 mm/min by using a universal material testing machine (Instron 5569/50K). A Brinell Rockwell & Vickers optical hardness tester (HBRVU−187.5) was used for microscopic Vickers hardness testing with a load of 0.98 N for 15 s. A dry sliding friction wear test was conducted at room temperature on a ball and disk friction wear tester (HT−1000). GCr15 steel balls with a hardness of HRC 55−66 were used as the counterface material. The parameters of the wear test were a load of 8 N, a rotation speed of 200 r/min, and a test time of 3600 s. After the test, the specimen was weighed, and the wear rate was calculated.

3 Results and discussion

3.1 Microstructure of plates with adsorbed amorphous carbon

Figure 2 shows the surface morphologies and C element distributions of the A6061 aluminum

alloy plates before and after the HTCAP process. It is evident that the pure plate surface is flat with parallel rolled streaks and no carbon element exists (Figs. 2(a, a_1, a_2)). After the HTCAP process, a uniform carbon film is generated on the surface of HTCAP-0.1 (Figs. 2(b, b_1, b_2)), which has a typical flocculent morphology. When the glucose solution concentration is increased, several monodisperse carbon spheres are randomly distributed on the surface of HTCAP-0.2 in addition to the coagulated carbon film, as shown in Figs. 2(c, c_1, c_2)). When the glucose solution concentration reaches 0.3 mol/L, the carbon spheres gradually increase and locally aggregate on the surface of HTCAP-0.3. Meanwhile, the carbon film gradually becomes dense (Figs. 2(d, d_1, d_2)). When the glucose solution concentration is further increased to 0.4 mol/L, the aggregation of carbon spheres becomes obvious. Furthermore, the monodisperse carbon spheres closely cross-link with each other, and the carbon is gradually enriched, leading to a decrease in carbon dispersion, as shown in Figs. 2(e, e_1, e_2).

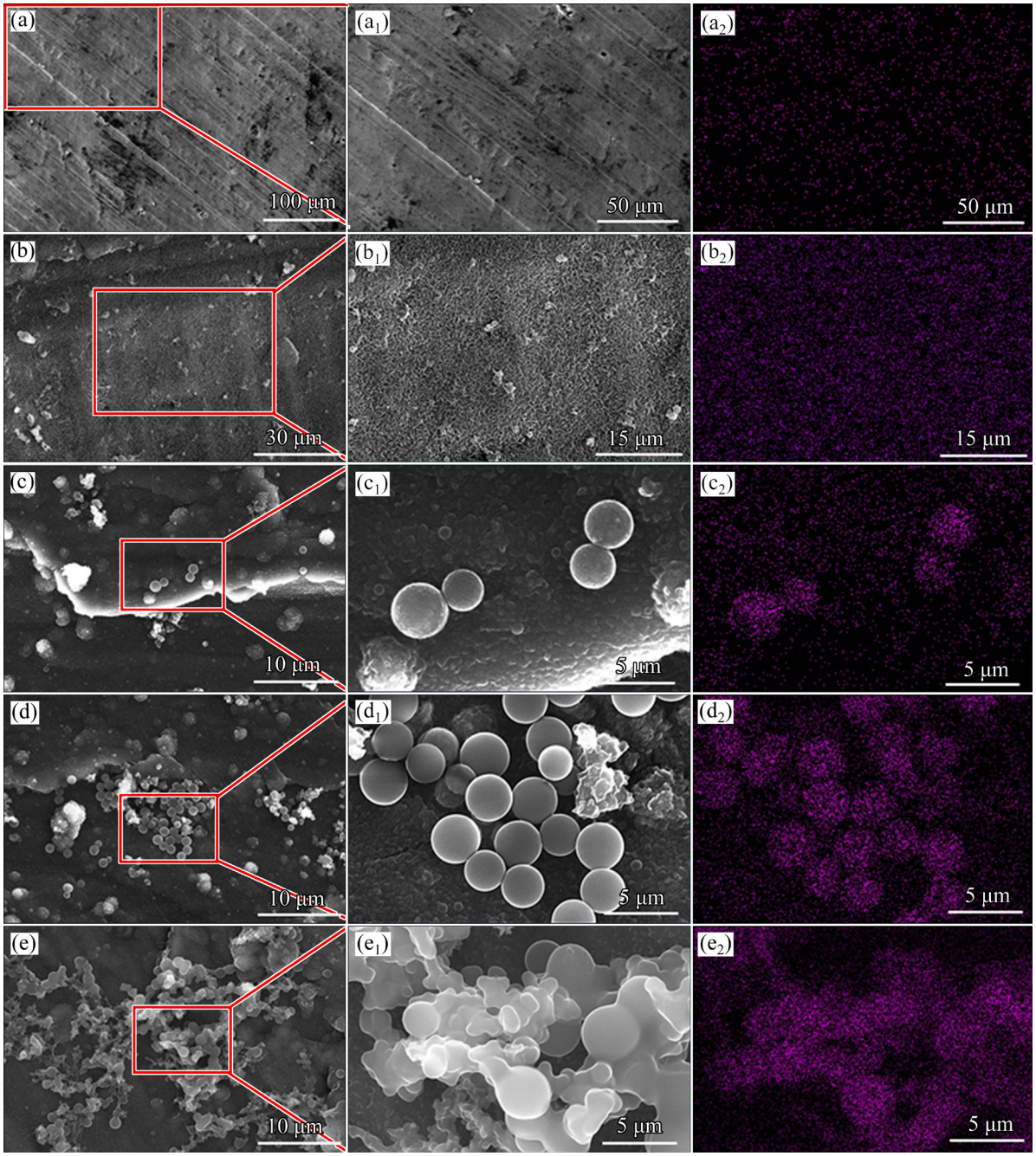

Fig. 2 SEM micrographs (a−e, a_1−e_1) and C element distribution (a_2−e_2) of A6061 plates: (a, a_1, a_2) Pure plate; (b, b_1, b_2) HTCAP-0.1; (c, c_1, c_2) HTCAP-0.2; (d, d_1, d_2) HTCAP-0.3; (e, e_1, e_2) HTCAP-0.4

To determine the structure of carbon on the surface of the A6061 plates, Raman spectroscopy was performed on the A6061 plate surface after the HTCAP process. As shown in Fig. 3, the D-band (at approximately 1361 cm^{-1}) and the G-band (at approximately 1591 cm^{-1}) are observed in the Raman spectra, which are typical spectra of amorphous carbon (APC). Meanwhile, as the glucose solution concentration increases from 0.1 to 0.4 mol/L, the intensities of the D peak and G peak apparently increase, indicating that the carbon content increases on the surface of the plate. Moreover, the peak intensity ratios (I_D/I_G) are 0.85, 0.73, 0.62 and 0.52, respectively. It is suggested that the graphitization of carbon gradually increases with increasing glucose solution concentration. All the peak intensity ratios (I_D/I_G) are greater than 0.52, so the carbon structure is still dominated by APC.

The HTCAP-0.1 and HTCAP-0.3 were ultrasonically treated for 15 min in an alcohol solution. The carbon/alcohol suspensions were dropped onto a 300-mesh copper grid for TEM analysis. The TEM morphology, HRTEM images and formation process of APC on the surface of the A6061 plates are shown in Fig. 4. The carbon film on the surface of HTCAP-0.1 has a flocculent-like structure (Fig. 4(a)), and HRTEM image (Fig. 4(b)) further proves that the carbon film is APC. With

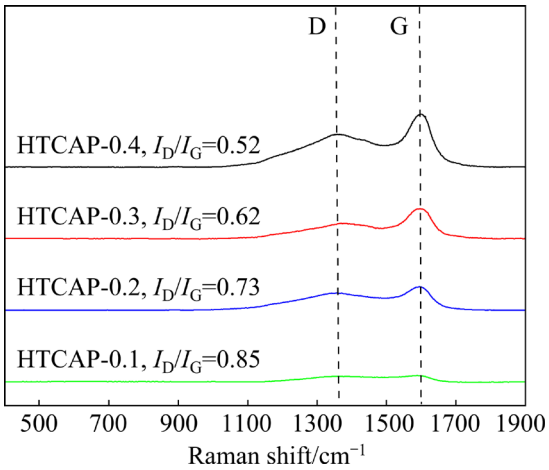

Fig. 3 Raman spectra of A6061 plates after HTCAP process

increasing the glucose solution concentration, both the carbon sphere and a carbon film with an amorphous structure coexist on the surface of HTCAP-0.3, as shown in Fig. 4(c). The carbon sphere has a dense carbon core with a flocculent edge (carbon film), as shown in Fig. 4(d), which further confirms that the carbon spheres are formed from the growth of the carbon film. Thus, the carbon spheres and the carbon film are tightly linked, and the carbon spheres can closely adsorb on the surface of the A6061 plate.

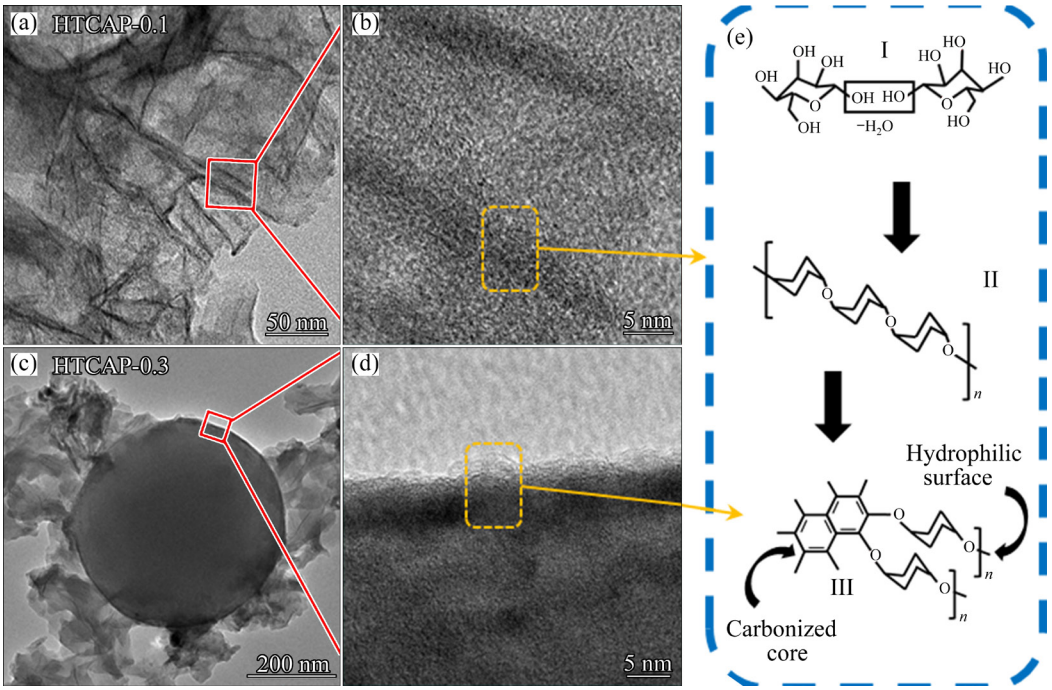

Fig. 4 TEM images (a, c) and HRTEM images (b, d) of APC on surface of A6061 plates and schematic diagram of APC formation process (e)

The hydrothermal reaction of glucose solutions is generally considered to be consistent with the growth mechanism of the LaMer model [25]. When the glucose solution concentration is low, the glucose molecules form large molecules of aromatic compounds and oligosaccharide carbon chains with a flocculent-like structure through dehydration and polymerization, which is Stage II of the APC formation process during the hydrothermal carbonization reaction (Fig. 4(e)). Moreover, the formed aromatic compounds and oligosaccharide carbon chains can easily adsorb onto the surface of aluminum alloy plates because they are rich in oxygen-containing functional groups. As the glucose solution concentration increases, the content of aromatic compounds and oligosaccharide carbon chains tends to saturate at random positions of the carbon film, and they will further dehydrate, cross-link and condense to form carbon nuclei. Subsequently, the carbon nuclei grow up into carbon spheres by further absorbing the surrounding aromatic compounds and oligosaccharide carbon chains. In contrast, the rest of the carbon film still exists as the growth substrate of carbon spheres, which is Stage III of the APC formation process (Fig. 4(e)). When the glucose solution concentration further increases, the aromatic compounds and oligosaccharide carbon chains are more likely to reach the saturation concentration, and the carbon nuclei significantly increase, causing carbon spheres to gradually increase and cross-link with one another.

3.2 Microstructure of APC/Al laminated composites

Figure 5 shows the optical microscopy microstructures of the APC/Al laminated composites in the hot-press direction. The thick light-colored layers in the composites are the matrix A6061 alloy, the thin dark-colored interlayers are mainly composed of APC, and the enlarged area in the red box highlights the interfacial morphology features of the APC/Al laminated composites. The interlayer of composites prepared from pure plates has a typical jagged shape (Fig. 5(a)), reflecting the mechanical bond caused by the plastic deformation of the A6061 alloy during the hot-press sintering process. After the HTCAP process, the APC/Al laminated composites have flat and continuous interlayers (Figs. 5(b−d)), indicating that APC can hinder plastic deformation of the matrix A6061 alloy. As the glucose solution concentration increases, the average interlayer thickness gradually increases, as shown in Fig. 5(f). When the glucose solution concentration reaches 0.4 mol/L (Fig. 5(e)), the interlayers become discontinuous and uneven in thickness, demonstrating that APC distributes inhomogeneously due to agglomeration of APC.

Figure 6 shows SEM micrographs and element distributions of the laminated composites prepared from pure plates and HTCAP-0.3. A slender gap exists in the interlayer of the laminated composites prepared from pure plates, while the interlayer of the APC/Al laminated composites prepared from HTCAP-0.3 is filled, as shown in Figs. 6(a, b). It is

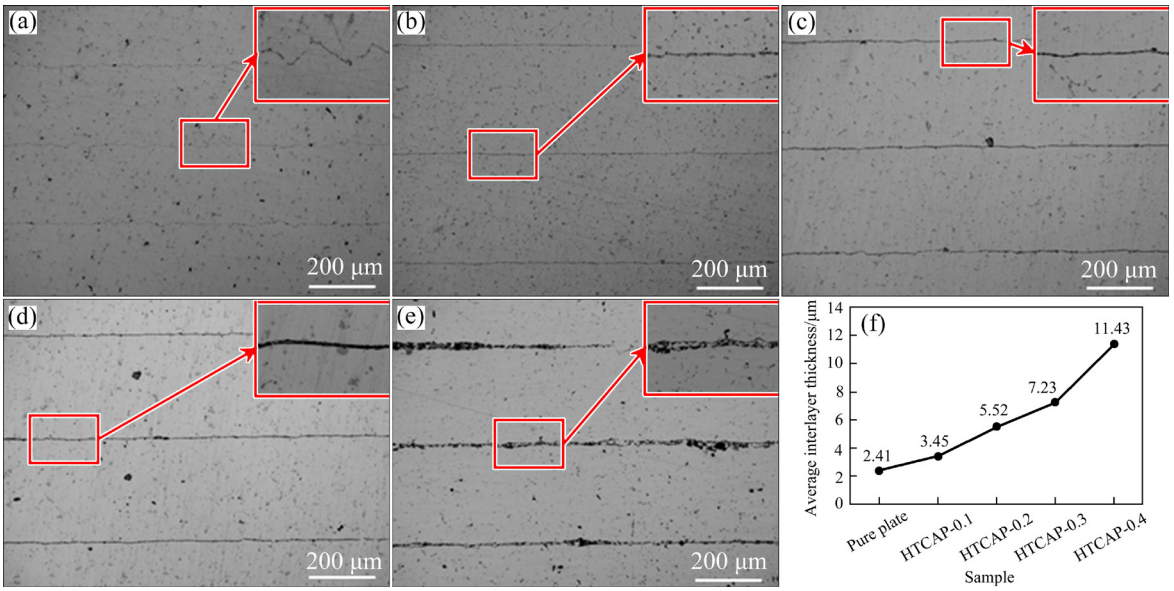

Fig. 5 Microstructures (a−e) and average interlayer thickness (f) of APC/Al laminated composites prepared from A6061 plates: (a) Pure plate; (b) HTCAP-0.1; (c) HTCAP-0.2; (d) HTCAP-0.3; (e) HTCAP-0.4

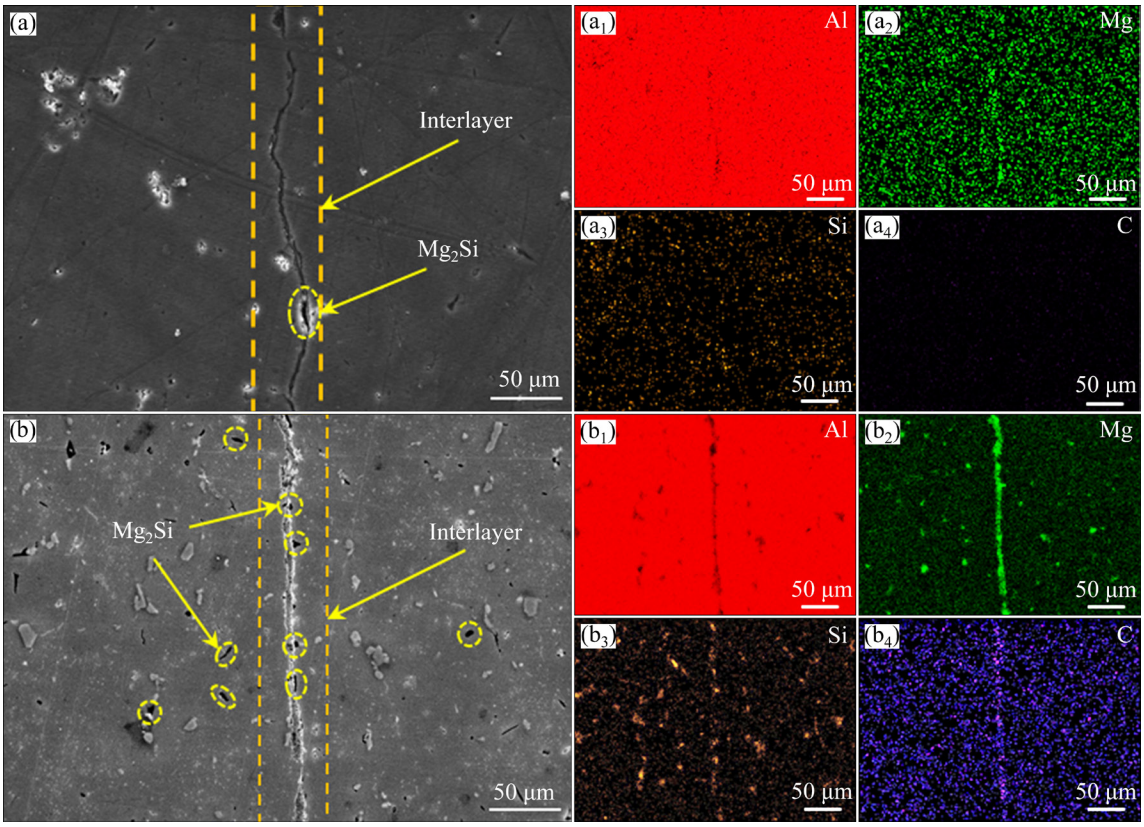

Fig. 6 SEM micrographs (a, b) and element distributions (a_1−a_4, b_1−b_4) of APC/Al laminated composites prepared from A6061 plates: (a, a_1−a_4) Pure plate; (b, b_1−b_4) HTCAP-0.3

further confirmed from the element distributions that APC is mainly distributed along the interlayer of the APC/Al laminated composites (Fig. 6(b_4)), which is consistent with the result of Fig. 5. Moreover, Mg element also obviously enriches in the interlayer of the APC/Al laminated composites, and Si element agglomerates both in the interlayer and on the A6061 plate, suggesting that Mg atoms and Si atoms seriously precipitate and form Mg_2Si phase during the HTCAP process.

The XRD patterns of the APC/Al laminated composites are shown in Fig. 7. The A6061 alloy mainly consists of α(Al) and Mg_2Si phases. The diffraction peaks of Al and Mg_2Si can be clearly detected in all the APC/Al laminated composites after the HTCAP process. However, the diffraction peaks of Mg_2Si are indistinct for the laminated composites prepared from pure plates in comparison, which is in agreement with the SEM result in Fig. 6(a). Thus, it is concluded that most of the Mg_2Si phase precipitates during the hydrothermal reaction. Additionally, the diffraction peaks of APC are difficult to distinguish. The diffraction angle area from 18° to 30° is magnified,

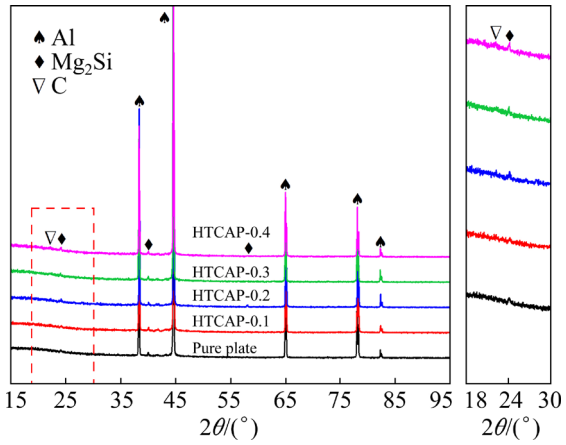

Fig. 7 XRD patterns of APC/Al laminated composites

and the peaks corresponding to APC are observed at approximately 24° in all the APC/Al laminated composites. Moreover, the intensity of the APC peaks becomes stronger as the glucose solution concentration increases, indicating that the content of APC in the APC/Al laminated composites increases.

To further reveal the interfacial bonding of APC and the matrix in the APC/Al laminated composites, TEM analyses were performed on the

APC/Al laminated composites prepared from HTCAP-0.3, as shown in Fig. 8. It is obvious that there is a diffusion zone between Al and APC at the interface, and Al and APC are uniformly distributed in the diffusion zone without voids or reaction products (Figs. 8(a, b)). The selective area electron diffraction (SAED) pattern shows the typical concentric diffraction rings, which can further demonstrate the amorphous carbon structure, as shown in Fig. 8(b_2). Figure 8(c) shows the TEM morphology of the center region of the interlayer. APC and Al are well bonded by the diffusion of Al, which is marked by the red dashed box in Fig. 8(c). The HRTEM image shows that APC is wrapped by Al, and there is still a diffusion region, as shown in Fig. 8(d). Through Fourier transform of the diffuse area, a diffraction pattern with the coexistence of spots and concentric diffraction rings is obtained (Fig. 8(d_1)), which is further processed into Fig. 8(d_2). The calibrated diffraction spots match those of Al, and the concentric diffraction rings agree with those of APC. Therefore, good interfacial bonding between APC and Al is achieved by the diffuse distribution of APC and Al, which can provide the basis to improve the mechanical and tribological performance.

3.3 Mechanical properties of APC/Al laminated composites

Figure 9 shows the matrix hardness, interlayer hardness and location of sampling points of the laminated composites. The matrix hardness of the laminated composites is constant, approximately HV 48.53. The interlayer hardness of the laminated composites prepared from pure plates is approximately HV 50.57. After the plates are treated by the HTCAP process in glucose solution (0.1 mol/L), the interlayer hardness of the APC/Al laminated composite significantly increases to the maximal value (HV 55.53). This is mainly generated by the aggregated distribution of the Mg_2Si phase in the interlayer during the hydrothermal reaction, as evidenced by the interlayer enrichment of elemental Mg and Si in Fig. 6. Moreover, as the glucose solution concentration increases, the interlayer hardness of the APC/Al laminated composites gradually decreases. Among them, the interlayer hardness of the APC/Al laminated composites prepared from HTCAP-0.4 is the lowest (approximately HV 49.91), even less than that of the sample prepared from pure plates, which is primarily attributed to the low hardness of APC. The greater the glucose solution concentration

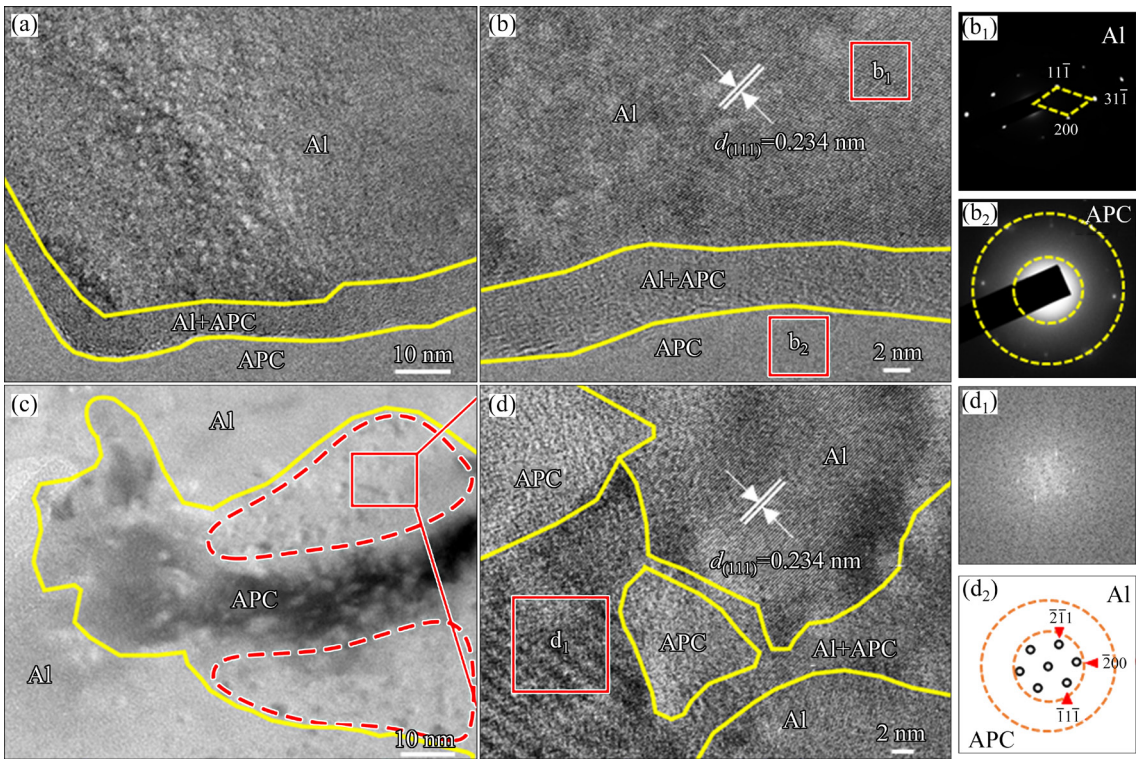

Fig. 8 TEM images (a, c), HRTEM images (b, d) and SAED patterns (b_1, b_2, d_1, d_2) of APC/Al laminated composites prepared from HTCAP-0.3: (a, b, b_1, b_2) Composites interface; (c) Center region of composites interlayer

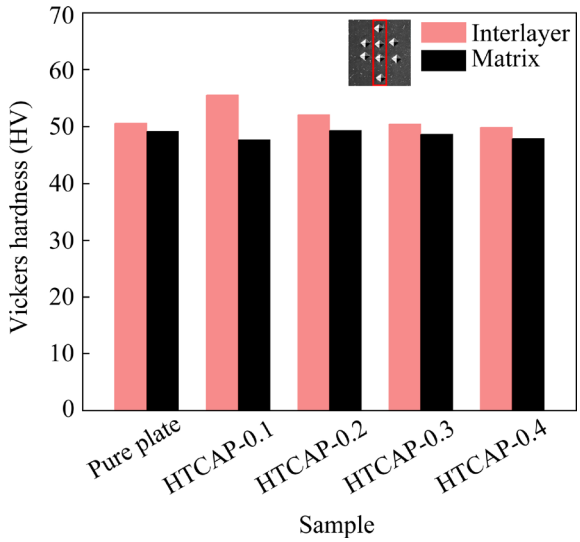

Fig. 9 Hardness of APC/Al laminated composites

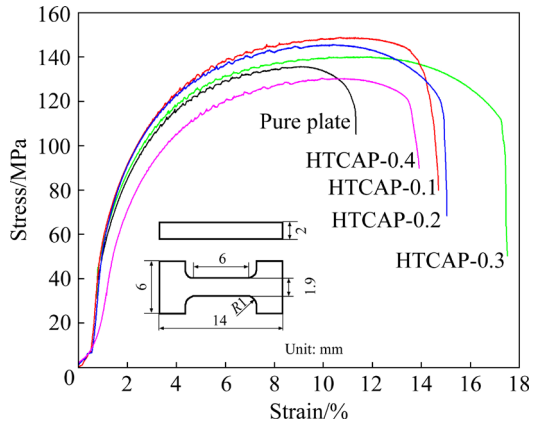

Fig. 10 Stress−strain curves of APC/Al laminated composites

is, the greater the content of APC is, and the lower the interlayer hardness is.

The tensile properties of the APC/Al laminated composites were also further investigated, as shown in Fig. 10. The ultimate tensile strength (UTS) and elongation (EL) present the same trend as the interlayer hardness, and videlicet, they increase firstly and then decrease as the glucose solution concentration increases. Compared to the laminated composites prepared from pure plates (135.78 MPa and 11.5%), the UTS and EL of the APC/Al laminated composites significantly increase. The highest UTS and EL are 148.91 MPa (HTCAP-0.1) and 16.4% (HTCAP-0.3), with improvements of 9.6% and 42.6%, respectively. Although it has low hardness and strength, APC could effectively fill the gap between the interlayers and densify the composites, leading to elimination of cracks. Furthermore, good interfacial bonding between APC and Al is achieved by the diffusion of Al, resulting in the formation of a continuous plastic deformation gradient zone coordinating with the matrix and the interlayers. During the tensile process, the APC film plays an important role in releasing tensile stress and improving plasticity. Thus, the tensile properties of APC/Al laminated composites, especially the elongation, are remarkably improved. However, with a further increase in glucose solution concentration, the agglomeration of APC causes deterioration of interfacial bonding and a decrease in the tensile properties.

3.4 Tribological properties of APC/Al laminated composites

The tribological properties, including the coefficient of friction (COF) and wear rate, of the laminated composites were measured. The friction test curves and variations in the COF and wear rate with the glucose solution concentration are shown in Fig. 11. The COF and wear rate of the laminated composites prepared from pure plates are the largest (0.46 and 1.01×10^{-5} mm^3/(N·m), respectively), and the COF−time curve greatly fluctuates, indicating that the wear surface is rough. After the HTCAP process, the COF of APC/Al laminated composites gradually decreases, and the COF−time curves become smooth with increasing glucose solution concentration, while the wear rate first decreases and then increases. The minimum COF (0.376) and minimum wear rate (0.344×10^{-5} mm^3/(N·m)) are achieved for the samples prepared from HTCAP-0.4 and HTCAP-0.3, respectively, which are reduced by 18.26% and 65.94% compared with those of the laminated composites prepared from pure plates. This mainly occurs because the APC in the interlayer is crushed into APC lubrication film, covering the surface of APC/Al laminated composites during sliding friction, and the APC film can effectively hinder direct contact between the wear surfaces and significantly enhance the wear resistance. However, when the glucose solution concentration is further increased to 0.4 mol/L, the wear rate increases, and the COF−time curve becomes volatile again. The aggregation of APC in the interlayers affects the interfacial bonding of the composites and deteriorates the tribological properties.

Figure 12 shows the SEM morphologies of the wear surfaces of the laminated composites. In addition to some microcracks, severe delamination appears on the surface of the laminated composites prepared from pure plates, which is a typical characteristic of adhesive wear [26], as shown in

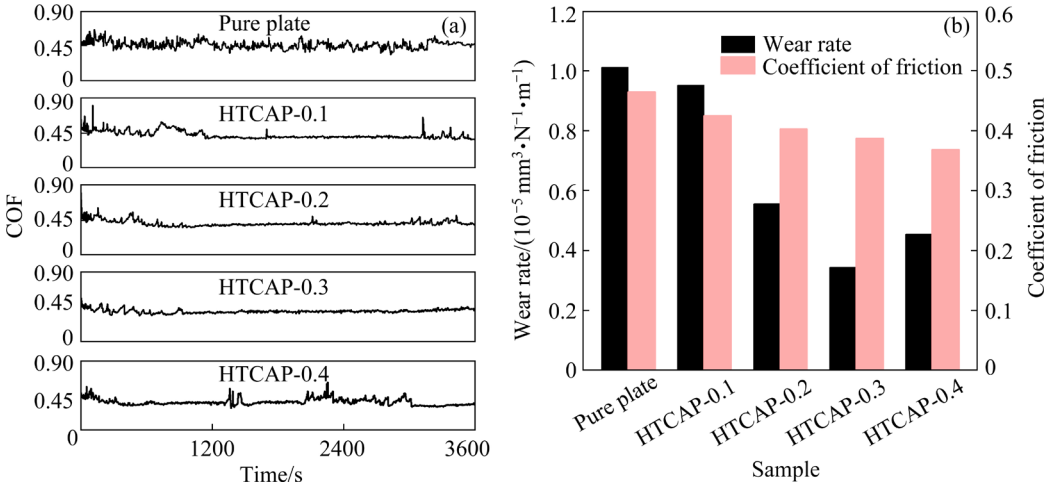

Fig. 11 Friction test curves (a), and COF and wear rate (b) of APC/Al laminated composites

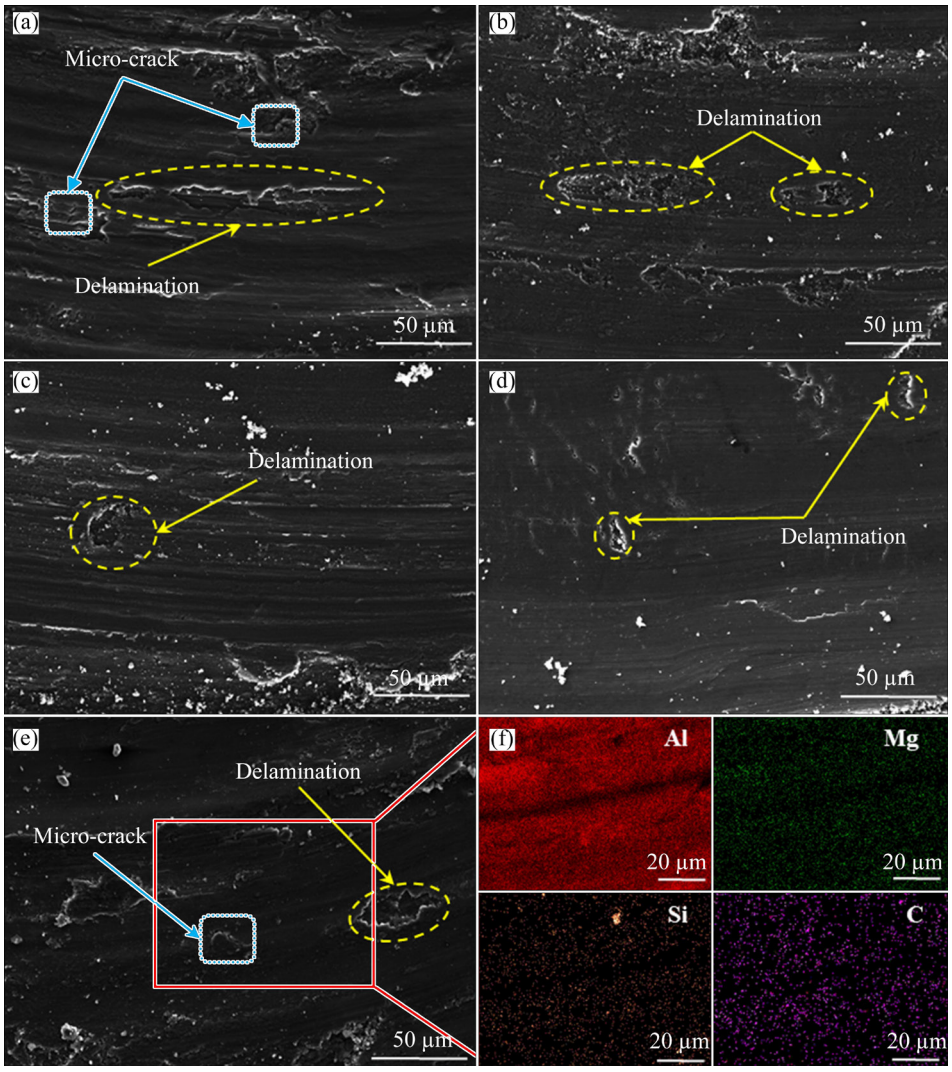

Fig. 12 SEM micrographs of wear surfaces of APC/Al laminated composites prepared from A6061 plates: (a) Pure plate; (b) HTCAP-0.1; (c) HTCAP-0.2; (d) HTCAP-0.3; (e) HTCAP-0.4; (f) Element distributions of HTCAP-0.4

Fig. 12(a). Thus, the dominant wear mechanism is adhesive wear caused by the direct contact between the sample and the steel ball under the normal force and shear force during sliding, leading to higher COF and wear rate. When the APC formed during the hydrothermal reaction is introduced into the laminated composites, although adhesive wear still plays the dominant role, the delamination positions and delamination sizes on the wear surface of the APC/Al laminated composites gradually decrease with increasing glucose solution concentration, and the wear surface becomes smooth, corresponding to the lower COF and wear rate, as shown in Figs. 12(b−d). Due to the easy sliding of APC under shear stress, an APC film acting as a solid lubricant is generated on the wear surface of the matrix aluminum alloy (Fig. 12(f)). However, when the glucose solution concentration further increases to 0.4 mol/L, delamination and microcracks around the interlayer begin to increase (Fig. 12(e)) because APC significantly agglomerates in the interlayer of the APC/Al laminated composite, forming a softer area than the surrounding area. Therefore, adhesive wear is more likely to occur at the edge of the softer area.

A schematic diagram of the wear surface of the laminated composites is shown in Fig. 13. According to Archard's wear theory, the theoretical wear rate (W) of a material in dry sliding friction is expressed as [27,19]

$$W = \frac{kxp}{3H} \tag{1}$$

where k is the COF, x is the dry sliding friction distance, p is the applied normal load, and H is the hardness of the material. According to Eq. (1), theoretically, the wear rate is inversely proportional to the hardness and directly proportional to COF. However, in the actual process of friction and wear, when the glucose solution concentration increases in the range of 0−0.3 mol/L, the wear rate gradually decreases as the hardness of the laminated composites first increases and then decreases (Figs. 9 and 11(b)), which is mainly attributed to the formation of the APC lubrication film. In the sliding process of the steel ball, the laminated composites prepared from pure plates are directly in contact with the steel ball. The microcracks initiate at the matrix alloy, induced by a combination of stress and friction, and propagate through plastic deformation to form a stripping interface. Then, the debris entirely detaches from the wear surface, and delamination is formed, as shown in Fig. 13(a). Thus, the wear rate and COF of the laminated composites prepared from the pure plate are the largest.

After the introduction of APC, the APC in the APC/Al laminated composites separates and transfers to the surface of the aluminum matrix with the movement of the steel ball, forming a self-lubricating film (Fig. 13(b)) [28]. Since the APC lubrication film hinders direct contact between the APC/Al laminated composites and the steel ball, the wear rate and COF significantly decrease. When the glucose solution concentration further increases to 0.4 mol/L, a soft area with lower hardness is formed in the interlayers because of the agglomeration of APC. Under the normal force and shear force during sliding, when the steel ball

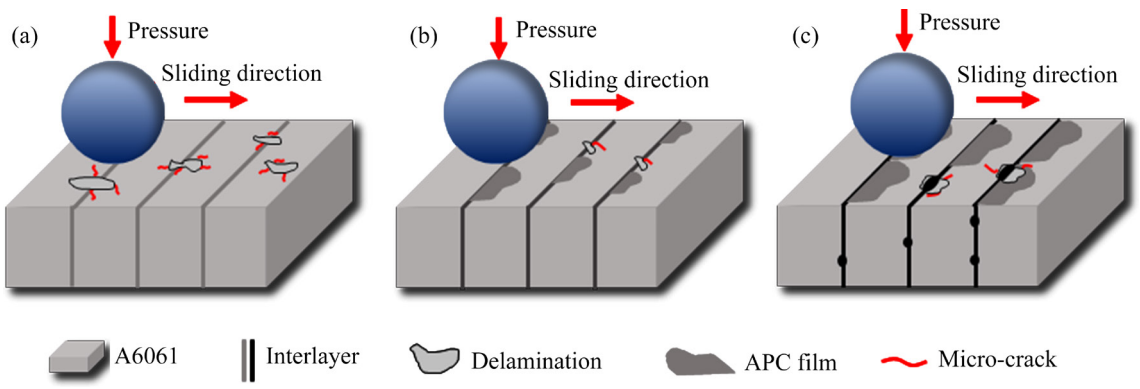

Fig. 13 Schematic diagram of wear surfaces of APC/Al laminated composites prepared from A6061 plates: (a) Pure plate; (b) HTCAP-0.3; (c) HTCAP-0.4

passes through the soft zone, the matrix alloy nearby is seriously impacted, resulting in micro-cracks. Therefore, new delamination and spalling surfaces emerge (Fig. 13(c)), and the wear rate increases once again.

4 Conclusions

(1) Novel laminated amorphous carbon (APC)/Al composites with excellent wear resistance are successfully prepared by the hydrothermal carbon adsorption on plates (HTCAP) and vacuum hot-press sintering (VHPS) process.

(2) During the HTCAP process, an APC film and APC spheres are formed from the dehydration and polymerization of glucose. They can adsorb on the surface of the aluminum plate through its rich oxygen-containing functional groups. After the VHPS process, APC is uniformly distributed in the interlayers and has good interfacial bonding with the matrix through the diffusion of Al.

(3) The interlayer hardness, ultimate tensile strength and elongation of the APC/Al laminated composites first increase and then decrease with increasing glucose solution concentration. Compared to the laminated composites prepared from pure plates, the interlayer hardness and ultimate tensile strength reach maximum values of HV 55.53 and 148.91 MPa, with improvements of 9.6% and 9.8%, respectively, when the glucose solution concentration is 0.1 mol/L. A maximum elongation of 16.4% is achieved, corresponding to an increase of 42.6%, at a glucose solution concentration of 0.3 mol/L.

(4) The coefficient of friction gradually decreases while the wear rate first decreases and then increases with increasing glucose solution concentration. Compared to laminated composites prepared from pure plates, the wear rate reaches the minimum value of 0.344×10^{-5} mm^3/(N·m), decreased by 65.94%, when the glucose solution concentration is 0.3 mol/L. A minimum coefficient of friction of 0.376 is achieved, with a decrease of 18.26%, at a glucose solution concentration of 0.4 mol/L.

(5) The dominant wear mechanism of the APC/Al laminated composites is adhesive wear. The improvement in wear resistance is attributed to the formation of a uniform APC lubrication film on the wear surface.

CRediT authorship contribution statement

Yi-han CHEN: Formal analysis, Investigation, Writing – Review & editing; **Hong-yu XU:** Data curation, Formal analysis, Investigation, Writing − Original draft, Funding acquisition, Conceptualization; **Bo JIANG:** Formal analysis, Writing – Review & editing; **Ye WANG:** Supervision; **Mao-liang HU:** Supervision; **Ze-sheng JI:** Conceptualization.

Declaration of competing interest

The authors declare that they have no known competing financial interests or personal relationships that could have appeared to influence the work reported in this paper.

Acknowledgments

This work was financially supported by the National Natural Science Foundation of China (No. 51704087), and the Natural Science Foundation of Heilongjiang Province, China (No. LH2020E083).

References

[1] WANG Xiang-dong, LIU Xiong, DING Hao, YAN Su-rong, XIE Zi-hua, PAN Bai-qing, LI Yong-hong, PAN Qing-lin, DENG Yun-lai, WANG Wei-yi. Microstructure and mechanical properties of Al−Mg−Si alloy U-shaped profile [J]. Transactions of Nonferrous Metals Society of China, 2020, 30(11): 2915−2926.

[2] LIU Tao, PEI Zong-rui, BARTON D, THOMPSON G B, BREWER L N. Characterization of nanostructures in a high pressure die cast Al−Si−Cu alloy [J]. Acta Materialia, 2022, 224: 117500.

[3] WENG Yao-yao, JIA Zhi-hong, DING Li-peng, LIAO Jin, ZHANG Ping-ping, XU Ya-qi, LIU Qing. Effect of pre-straining on structure and formation mechanism of precipitates in Al−Mg−Si−Cu alloy [J]. Transactions of Nonferrous Metals Society of China, 2022, 32(2): 436−447.

[4] BARADESWARAN A, PERUMAL A E. Influence of B_4C on the tribological and mechanical properties of Al 7075−B_4C composites [J]. Composites Part B−Engineering, 2013, 54: 146−152.

[5] ZHANG Z W, LIU Z Y, XIAO B L, NI D R, MA Z Y. High efficiency dispersal and strengthening of graphene reinforced aluminum alloy composites fabricated by powder metallurgy combined with friction stir processing [J]. Carbon, 2018, 135: 215−223.

[6] GUPTA R, NANDA T, PANDEY O P. Comparison of wear behaviour of LM13 Al−Si alloy based composites reinforced with synthetic (B_4C) and natural (ilmenite) ceramic particles [J]. Transactions of Nonferrous Metals Society of China, 2021, 31(12): 3613−3625.

[7] ARIF S, JAMIL B, SHAIKH M B N, AZIZ T, ANSARI A H, KHAN M. Characterization of surface morphology, wear performance and modelling of graphite reinforced aluminium

hybrid composites [J]. Engineering Science and Technology, an International Journal, 2020, 23(3): 674−690.

[8] PENG Xuan-yi, HUANG Ying, HAN Xiao-peng, FAN Rui, LIU Xu-dong. High volume fraction of copper coated graphite flake\Nitrogen doped carbon fiber reinforced aluminum matrix composites [J]. Journal of Alloys and Compounds, 2020, 822: 153584.

[9] CHANG Hao, SUN Jian, CHEN Guo-hong, WANG Bing, YANG Lei, ZHANG Jian-hua, TANG Wen-ming. Microstructure and properties of high-fraction graphite nanoflakes/6061Al matrix composites fabricated via spark plasma sintering [J]. Transactions of Nonferrous Metals Society of China, 2021, 31(6): 1550−1560.

[10] WANG Xue, XIAO Wei, WANG Jian-wei, SUN Lu, SHI Jing-min, GUO Hong, LIU Yan-qiang, WANG Li-gen. Enhanced interfacial strength of graphene reinforced aluminum composites via X (Cu, Ni, Ti)-coating: Molecular-dynamics insights [J]. Advanced Powder Technology, 2021, 32(7): 2585−2590.

[11] MUSTAFA O, BERNAB B. Study of microstructural, mechanical, thermal and tribological properties of graphene oxide reinforced Al−10Ni metal matrix composites prepared by mechanical alloying method [J]. Wear, 2022, 510/511: 204511.

[12] KHOSHGHADAM-PIREYOUSEFAN M, RAHMANIFARD R, OROVCIK L, ŠVEC P, KLEMM V. Application of a novel method for fabrication of graphene reinforced aluminum matrix nanocomposites: Synthesis, microstructure, and mechanical properties [J]. Materials Science and Engineering A, 2020, 772: 138820.

[13] XU Z Y, LI C J, GAO P, YOU X, BAO R, FANG D, TAO J M, YI J H. Improving the mechanical properties of carbon nanotubes reinforced aluminum matrix composites by heterogeneous structural design [J]. Composites Communications, 2022, 29: 101050.

[14] CHEN B, LI Z, SHEN J, LI S, JIA L, UMEDA J, KONDOH K, LI J S. Mechanical properties and strain hardening behavior of aluminum matrix composites reinforced with few-walled carbon nanotubes [J]. Journal of Alloys and Compounds, 2020, 826: 154075.

[15] ABBASIPOUR B, NIROUMAND B, MONIR VAGHEFI S M, ABEDI M. Tribological behavior of A356−CNT nanocomposites fabricated by various casting techniques [J]. Transactions of Nonferrous Metals Society of China, 2019, 29(10): 1993−2004.

[16] BARADESWARAN A, PERUMAL A E. Wear and mechanical characteristics of Al 7075/graphite composites [J]. Composites Part B, 2014, 56: 472−476.

[17] MAURYA R, KUMAR B, ARIHARAN S, RAMKUMAR J, BALANI K. Effect of carbonaceous reinforcements on the mechanical and tribological properties of friction stir processed Al6061 alloy [J]. Materials & Design, 2016, 98: 155−166.

[18] BASTWROS M M H, ESAWI A M K, WFIF A. Friction and wear behavior of Al−CNT composites [J]. Wear, 2013, 307(1/2): 164−173.

[19] HE Ying-jie, XU Hong-yu, HU Mao-liang, JIANG Bo, JI Ze-sheng. Effect of glucose concentrations on wear resistance of Al/APC composites prepared by hydrothermal carbonized deposition on chips [J]. Journal of Materials Science & Technology, 2020, 53: 82−90.

[20] ZHANG Bin-bin, WANG Jia, ZHANG Jie. Bio-inspired one-step hydrothermal fabricated superhydrophobic aluminum alloy with favorable corrosion resistance [J]. Colloids and Surfaces A: Physicochemical and Engineering Aspects, 2020, 589: 124469.

[21] ZHU Xiang-dong, LIU Yu-chen, ZHOU Chao, LUO Gang, ZHANG Shi-cheng, CHEN Jian-min. A novel porous carbon derived from hydrothermal carbon for efficient adsorption of tetracycline [J]. Carbon, 2014, 77: 627−636.

[22] HE Ying-jie, XU Hong-yu, JIANG Bo, HU Mao-liang, JI Ze-sheng. Microstructure, mechanical and tribological properties of (APC+B_4C)/Al hybrid composites prepared by hydrothermal carbonized deposition on chips [J]. Journal of Alloys and Compounds, 2021, 888: 161578.

[23] HE Ying-jie, XU Hong-yu, LIU Yang, CHEN Yi-han, JI Ze-sheng. Strengthening mechanism of B_4C@APC/Al matrix composites reinforced with bimodal-sized particles prepared by hydrothermal carbonized deposition on chips [J]. Journal of Materials Science & Technology, 2022, 123: 60−69.

[24] LI Zan, GUO Qiang, LI Zhi-qiang, FAN Gen-lian, XIONG Ding-Bang, SU Yi-shi, ZHANG Jie, ZHANG Di. Enhanced mechanical properties of graphene (reduced graphene oxide)/aluminum composites with a bioinspired nanolaminated structure [J]. Nano Letters, 2015, 15(12): 8077−8083.

[25] LIU Jun-li, SHI Wen-xiong, NI Bing, YANG Yong, LI Shu-zhou, ZHUANG Jing, WANG Xun. Incorporation of clusters within inorganic materials through their addition during nucleation steps [J]. Nature Chemistry, 2019, 11(9): 839−845.

[26] SHARMA A, SHARMA V M, PAUL J. A comparative study on microstructural evolution and surface properties of graphene/CNT reinforced Al6061-SiC hybrid surface composite fabricated via friction stir processing [J]. Transactions of Nonferrous Metals Society of China, 2019, 29(10): 2005−2026.

[27] ARCHARD J F. Contact and rubbing of flat surfaces [J]. Journal of Applied Physics, 1953, 24(8): 981−988.

[28] TONG Yun-qi, LI Wei, SHI Qiu-sheng, CHEN Lin, YANG Guan-jun. Self-lubricating epoxy-based composite abradable seal coating eliminating adhesive transfer via hierarchical design [J]. Journal of Materials Science & Technology, 2022, 104: 145−154.

铝板水热碳吸附工艺制备 APC/Al 层状复合材料的显微组织、力学性能和摩擦学性能

陈奕涵[1]，许红雨[1,2]，姜 博[1]，王 晔[1]，胡茂良[1]，吉泽升[1]

1. 哈尔滨理工大学 材料科学与化学工程学院，哈尔滨 150080；
2. 哈尔滨理工大学 先进制造智能化技术教育部重点实验室，哈尔滨 150080

摘 要：采用铝板水热碳吸附工艺(HTCAP)和真空热压烧结工艺(VHPS)制备无定形碳(APC)/Al 层状复合材料，研究葡萄糖溶液浓度对其显微组织、力学性能和摩擦学性能的影响。结果表明，APC 在层间分布均匀，并且通过 Al 的扩散与基体形成良好的界面结合。随着葡萄糖溶液浓度的增加，层间硬度、极限抗拉强度(UTS)和伸长率先增大后减小，而磨损率则呈现相反的趋势，摩擦因数(COF)逐渐减小。当葡萄糖溶液浓度为 0.3 mol/L 时，伸长率最大，为 16.4%，磨损率最小，为 0.344×10^{-5} $mm^3/(N\cdot m)$。粘着磨损是 APC/Al 层状复合材料的主要磨损机制。耐磨性的提高是由于在磨损表面形成均匀的 APC 润滑膜。

关键词：铝基层状复合材料；无定形碳；水热反应；界面显微组织；摩擦学性能

(Edited by Bing YANG)